nature chemistry

ARTICLES

PUBLISHED ONLINE: 18 APRIL 2016 | DOI: 10.1038/NCHEM.2487

Chemical polyglycosylation and nanolitre detection enables single-molecule recapitulation of bacterial sugar export

Lingbing Kong[1], Andrew Almond[2], Hagan Bayley[1]* and Benjamin G. Davis[1]*

The outermost protective layer of both Gram-positive and Gram-negative bacteria is composed of bacterial capsular polysaccharides. Insights into the interactions between the capsular polysaccharide and its transporter and the mechanism of sugar export would not only increase our understanding of this key process, but would also help in the design of novel therapeutics to block capsular polysaccharide export. Here, we report a nanolitre detection system that makes use of the bilayer interface between two droplets, and we use this system to study single-molecule recapitulation of sugar export. A synthetic strategy of polyglycosylation based on tetrasaccharide monomers enables ready synthetic access to extended fragments of K30 oligosaccharides and polysaccharides. Examination of the interactions between the *Escherichia coli* sugar transporter Wza and very small amounts of fragments of the K30 capsular polysaccharide substrate reveal the translocation of smaller but not larger fragments. We also observe capture events that occur only on the intracellular side of Wza, which would complement coordinated feeding by adjunct biosynthetic machinery.

Capsular polysaccharides (CPSs) are ubiquitous in both Gram-positive and Gram-negative bacteria. The CPS layer, as the outermost layer in bacteria, not only impedes macrophage and neutrophil-mediated phagocytosis, but also shields other cell surface effector molecules and prevents them from interacting with the host pattern recognition receptors and complement factors[1]. This means that CPS provides a key defensive layer for pathogens. Functional knowledge of CPS export (Fig. 1a) remains limited, despite the elegant determination of the structures and functions of the key components of the associated machinery[2–6], and acquiring the molecular details of the interaction between CPS and the transporter at the single-molecule level could therefore prove valuable. One barrier to this is the availability of pure, defined polysaccharide substrates, and a general approach for the synthesis of complex oligosaccharides (with potential extension to functional polysaccharides[7–10]) has remained a critical need[11–13].

Here, we reveal a generalized polysaccharide synthesis strategy that addresses this challenge. This approach has been combined with a nanoscale transport protein sensor of export interactions. Together, these create a combined system to investigate CPS transport at the single-molecule level (Fig. 1).

K30 CPS is the branched polysaccharide found in *Escherichia coli* strain E69 (O9a:K30:H12). It is identical to the CPS of the *Klebsiella* K20 strains[14] and is composed of tetrasaccharide repeating units (Fig. 1b). To explore a generalized synthesis of pure K30 CPS fragments, we exploited a polymerization glycosylation (polyglycosylation[15]) approach using defined oligosaccharide precursors. We envisaged that suitably functionalized oligosaccharidic 'monomers', if suitably reactive at distinct termini, could be regioselectively polymerized (Fig. 1c). To our knowledge, such a strategy has rarely[16–18] been successfully employed before. In the case of K30, the approach required the chemical synthesis of partially protected tetrasaccharide repeating units that could then be further activated for polymerization and hence allow the collection of oligomers and polymers of the repeating units. Deprotection of the purified oligomers and polymers would then afford representative fragments of K30 CPS as substrates (Fig. 1c).

In Gram-negative bacteria, CPSs are transported to the cell surface by the membrane protein Wza, which is the exit translocon of the transport machinery. In *E. coli* strain E69, Wza is an octameric structure of 340 kDa that includes a novel eight-helix barrel, which spans the outer membrane[4]. In addition to *E. coli* and *Klebsiella* strains, many other Gram-negative bacterial species make use of Wza homologues as exporters of CPS. We have previously identified constitutively open Wza mutants that are useful for the screening of blockers; mutant ΔP106-A107 was most conductive and did not display gating[19]. ΔP106-A107 was therefore chosen for the present study (Fig. 1c). The planar bilayer system used in previous Wza studies (Supplementary Fig. 1) requires large amounts of substrate by virtue of the large compartment volumes. Droplet–interface–bilayer (DIB) systems[20–25] use much less substrate, in a lower volume (~200 nl), and can hence more readily access required concentrations. However, typical DIB systems[20–24] cannot maintain a protein pore such as Wza in a bilayer during the addition of an external substrate, so the determination of the activity of the same protein before and after the addition of a substrate is not currently possible. We reasoned that DIBs might allow sufficiently sensitive detection, even with the testing sugar substrates described here, if this key problem could be overcome. We thus demonstrate here a DIB system that allows the direct introduction of a substrate via fusion with a substrate droplet (Fig. 1c, step ix).

This report therefore describes a sugar-transport recapitulation strategy that combines (1) novel chemistry (a new polyglycosylation approach to produce K30 CPS fragments as substrates) and (2) novel biophysics (direct detection of the interaction between these substrates and a single membrane protein Wza) in a specifically designed DIB-fusion system (Fig. 1c).

[1]Department of Chemistry, University of Oxford, Chemistry Research Laboratory, Mansfield Road, Oxford OX1 3TA, UK. [2]School of Chemistry, Manchester Institute of Biotechnology, The University of Manchester, 131 Princess Street, Manchester M1 7DN, UK. *e-mail: hagan.bayley@chem.ox.ac.uk; ben.davis@chem.ox.ac.uk

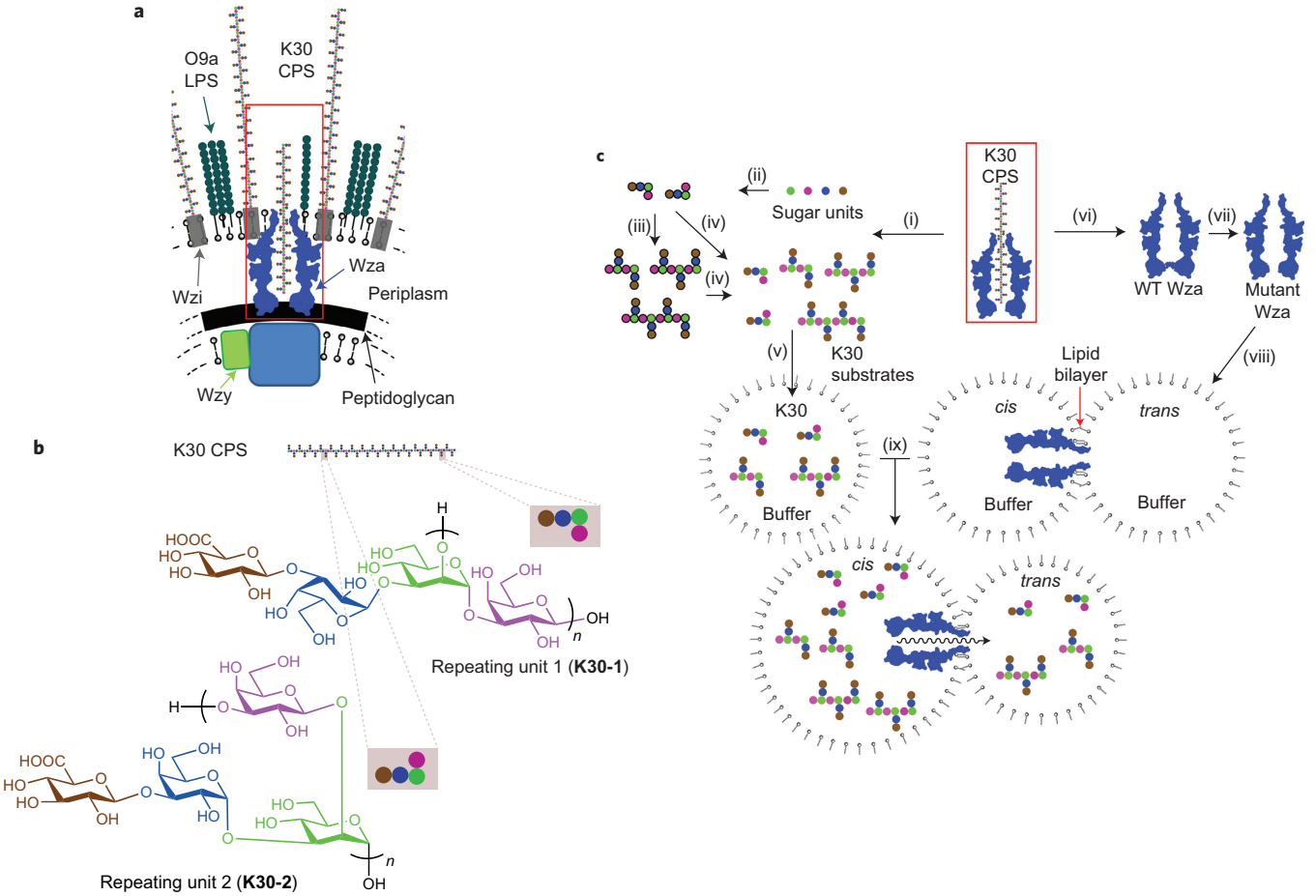

Figure 1 | Natural and recapitulated export of K30 CPS through the membrane protein Wza. a, Schematic of the structure of the cell surface in *E. coli* E69 and the associated machinery for K30 CPS export. The structure of a 16-repeating-unit fragment of K30 CPS was generated using SWEET2[19,41,42] and superimposed on the cross-sectional structure of wild-type Wza in PyMOL. This structure was used to generate the sphere 'cartoon' representation shown. The glycosyl units that make up K30 are represented by coloured spheres (green, α-D-mannosyl; magenta, β-D-galactosyl; blue, α-D-galactosyl; brown, β-D-glucuronyl). **b**, Chemical structure of K30 CPS. The two repeating oligosaccharidic units chosen as 'monomer' tetrasaccharides for polyglycosylation are shown highlighted by the grey boxes in the K30 polymer and are also drawn next to their corresponding structures (**K30-1** and **K30-2**). The glycosyl units are represented by coloured spheres (green, α-D-mannosyl; magenta, β-D-galactosyl; blue, α-D-galactosyl; brown, β-D-glucuronyl). **c**, A combined polyglycosylation and DIB-fusion strategy for the recapitulation of K30 sugar export through membrane protein Wza, allowing the detection of the Wza–sugar substrate interaction. Steps i to v represent a generalizable polyglycosylation synthetic strategy to create a defined polysaccharide substrate for analysis: (i) analysis of K30 CPS structures (see **b**); (ii) chemical synthesis of polymerizable partially protected repeating units of K30 CPS; (iii) polyglycosylation of polymerizable partially protected repeating units of K30 CPS; (iv) isolation and deprotection (represented by removal of sphere 'shells') of polysaccharides to afford representative K30 CPS fragments after separation; (v) formation of droplets containing fragments of K30 CPS suitable for analysis. Steps vi to viii represent the creation of a nanolitre single-molecule transport system: (vi) analysis of membrane protein Wza; (vii) protein engineering to afford constitutively open Wza pores; (viii) recapitulation of active Wza in a two-droplet bilayer (DIB) system. Step (ix) is the fusion of the K30 CPS fragment droplet (from step v) to either the *cis* or *trans* droplet of the DIB droplet pair. In the example shown, the *cis* droplet is fused with the substrate droplet, but the *trans* droplet could also be fused.

Results

Design of the synthesis of K30 polysaccharide. The structure of K30 CPS ($M_w \approx 150{,}000$, ~220 repeat units)[4,14] can be retrosynthetically broken down into two alternative 'monomer' tetrasaccharides (Fig. 1b). We hypothesized that the CPS polymer could be prepared by chemical polymerization (Fig. 1c, step iii) of these repeating units in partially protected and activated forms, **3** and **6** (Fig. 2). The polymers could then be isolated and deprotected (Fig. 1c, step iv) to afford the corresponding segments (**K30-1**$_n$ and **K30-2**$_n$, respectively) of the K30 polysaccharide. Importantly, this would test two complementary stereoselective strategies: the Ac group at C2 in **3** would allow neighbouring-group participation in polyglycosylation to afford Gal-β-selective polymeric products, and for **6**, stereoelectronically favoured axial delivery coupled with the steric effects of C2 and C3 glycosyl substituents would be expected to favour Man-α-selective polyglycosylation (Fig. 2). Therefore, both could potentially afford the desired –Gal-β-1,2–Man-α-1,3– repeating backbone structure.

A convergent '2+2' glycosylation strategy (Fig. 2) was chosen for the synthesis of both key building-block tetramers (the 'monomers' for polymerization), **3** and **6**, achieved by the reaction of trichloroacetimidate disaccharide donor units **4** or **7** with disaccharide acceptors **5** or **8**, respectively. Notably, selective activation of such trichloroacetimidate donors is possible in the presence of thioacetals. Hence, thioglycoside acceptors, which are themselves latent donors, could be used. In this way, a highly efficient route was developed, with a reduced need for functional-group interconversion to create active donors in later steps, while retaining an active moiety (the thioglycoside) ready for later polyglycosylation. We hypothesized that the desired α-stereoselectivity of this '2+2' glycosylation might be enabled

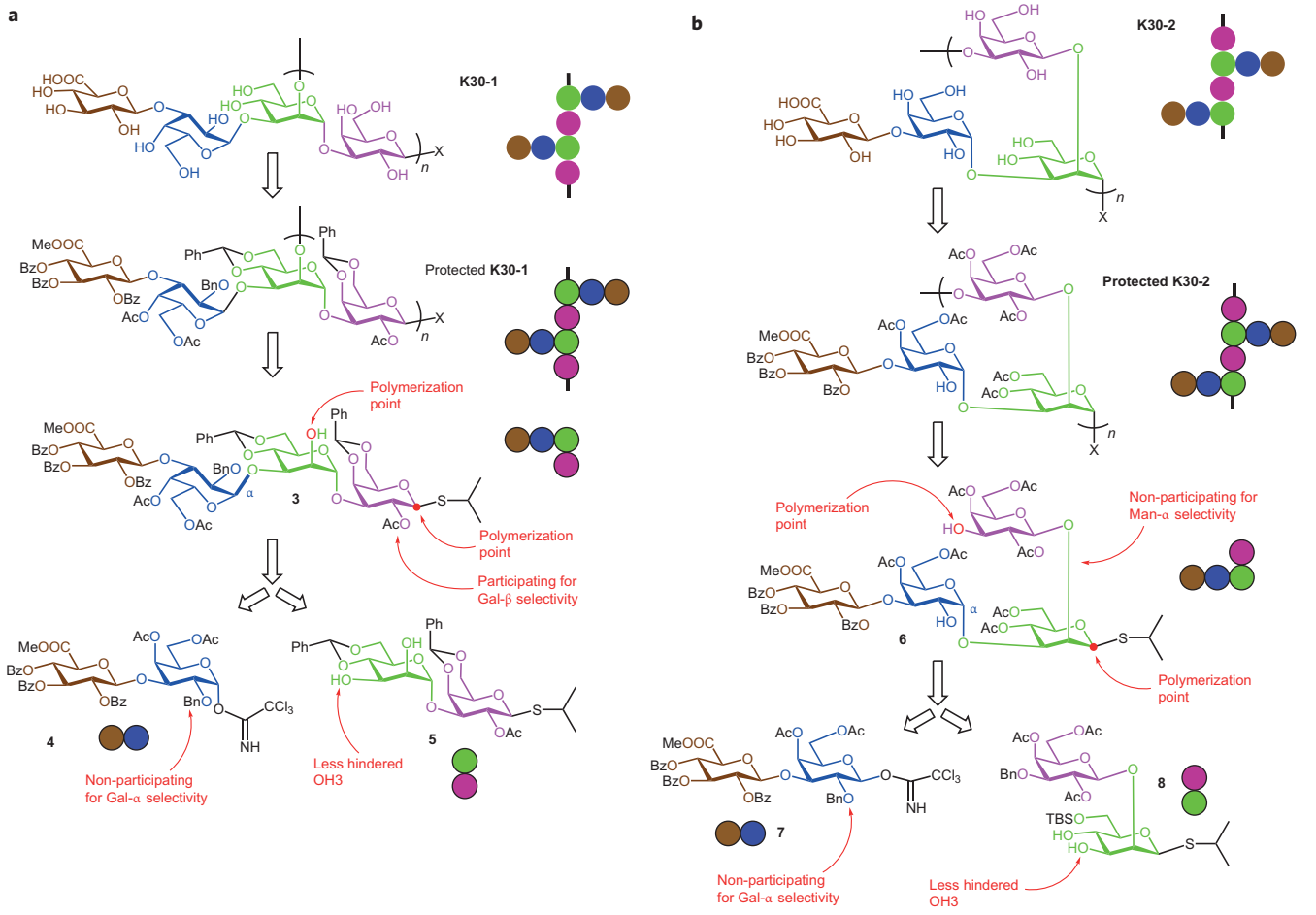

Figure 2 | Retrosynthetic analysis of K30 polysaccharide synthesis. a,**b**, Two repeating oligosaccharide units were chosen as 'monomers' for polyglycosylation. Tetrasaccharides **3** and **6** were chosen for the preparation of two K30 types: **K30-1** from **3** (**a**) and **K30-2** from **6** (**b**). These polymerizable repeating unit 'monomers' **3** and **6** were prepared using '2+2' glycosylation strategies, **4**+**5** and **7**+**8**, from disaccharide building blocks.

by a non-participating *O*-Bn group at the C2 position of the galactosyl unit of precursor disaccharide donors **4** and **7**, and this would allow construction of the –Gal-α-1,3–Man– linkage from both.

The acceptors for donors **4** and **7**, **5** and **8**, respectively, are only partially protected. Notably, for both, we chose a regioselective glycosylation method that would necessitate differentiation of one hydroxyl acceptor nucleophile over another. To build **3** from **4** and **5**, we reasoned that steric hindrance would lead to preferred glycosylation at the OH3 hydroxyl of **5**, not only due to the disfavoured axial orientation of the OH2 hydroxyl but also due to the adjacent steric bulk at *O*-1 of the galactopyranoside aglycon in **5**. Similarly, for the regioselectivity of the '2+2' glycosylation to form **6** from **7** and **8**, we hypothesized that steric hindrance would lead to glycosylation dominantly at the OH3 hydroxyl of **8** because the OH4 hydroxyl would be shielded by the bulky silyl ether (TBS) protecting group at *O*-6.

Finally, we also decided to make effective use of the S^{i}Pr thioglycoside moiety in the syntheses, not only to allow compatibility with trichloroacetimidates due to its predicted resistance to aglycon transfer[26,27] (enabling these acceptors to act as latent donors; see above) but also due to its ready manipulation as a hydrolysable C1 protecting group (allowing ready S^{i}Pr-to-OH conversion) as well as its widespread availability in key starting materials, such as IPTG (see next section).

Synthesis of disaccharide building blocks. The disaccharide building blocks were assembled first. Donor blocks **4** and **7** used a common synthetic route (Supplementary Fig. 2). As part of our strategy we used an unusual but readily available starting material for both Gal moieties, thiogalactoside **9**, which is also known as IPTG. The near ubiquitous use of this compound as a chemical inductant for *lac* operon-controlled protein expression in molecular biology suggested it as a useful resource. To allow selective access only to OH3 for glycosylation, OH4 and OH6 hydroxyls of **9** were protected by a benzylidene group[28] followed by formation of an *O*-Bn ether at OH2 under phase transfer catalysis (Fig. 3) to give **10**. The terminal glucuronyl (GlcA) was prepared[29] in suitably protected form as its methyl ester trichloroacetimidate donor **11** (ref. 29). GlcA donor **11** and Gal acceptor **10** were then coupled in good yield (84%) to afford GlcA-β-Gal disaccharide with excellent beta stereoselectivity (>98%). Subsequent protecting group manipulation (to improve stability under acidic conditions) via **12** allowed efficient thioglycoside hydrolysis to give access to both required disaccharide donors **4** and **7** (Fig. 3 and Supplementary Fig. 2). The trichloroacetimidate moiety in **4** and **7** was installed under conditions that gave a mixture of alpha and beta isomers (**4**/**7**), and these isomers were separated by chromatography.

The synthesis of disaccharide acceptor **5** (Figs 2 and 3) required to make **K30-1** necessitated the creation of another OH3-free Gal acceptor, but with critically different protection at *O*-2. Again, IPTG **9** was used as the starting material, but, unlike in the case of **10**, a participatory ester was required. Following benzylidene formation, as before, access to OH3 was achieved through a regioselective protecting group relay (Supplementary Fig. 3a). Bulky Fmoc was used first to cap OH3, allowing subsequent direct OH2 acetylation. Then, selective removal of Fmoc by the weak base

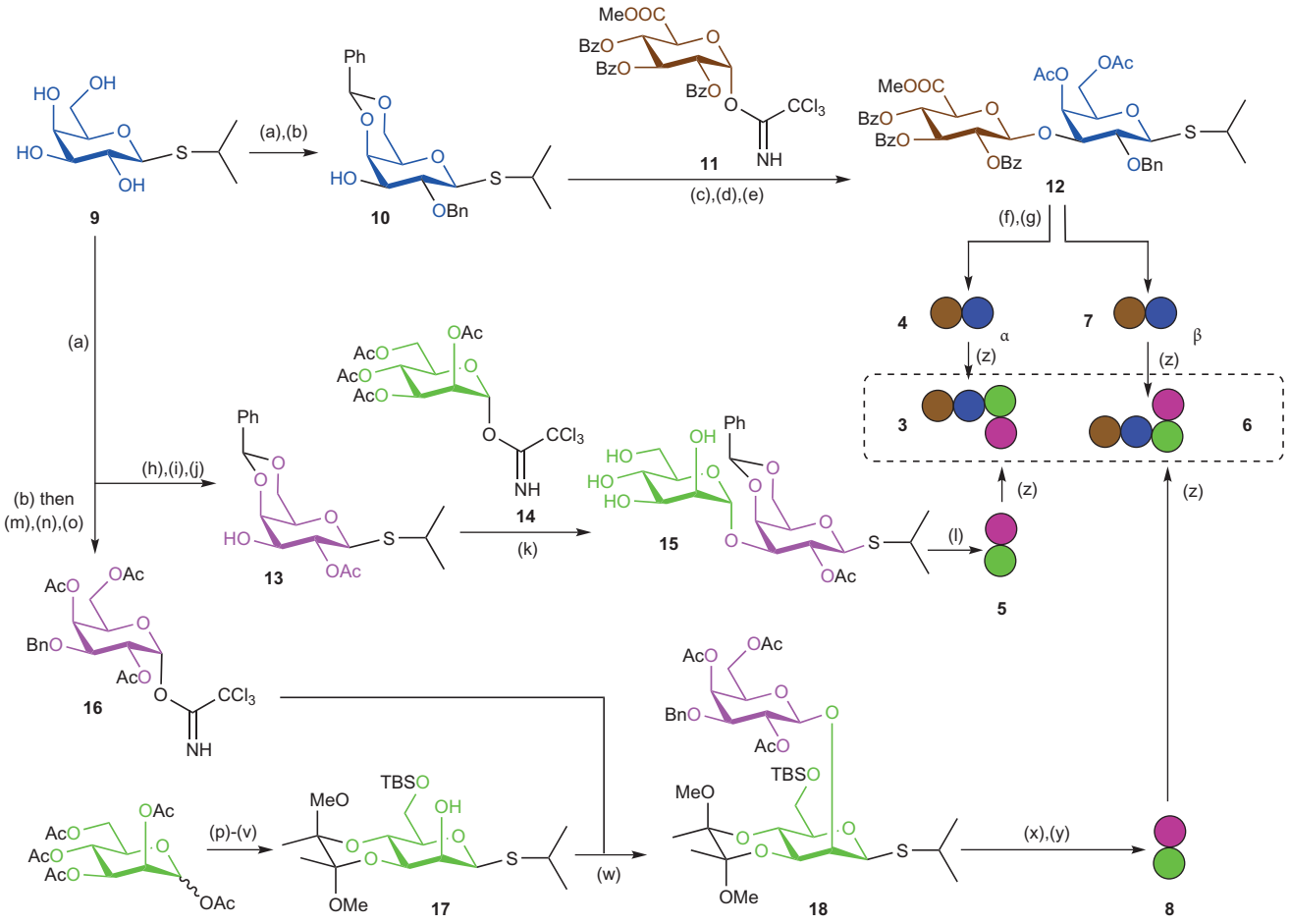

Figure 3 | Synthesis of disaccharide building blocks 4+5 and 7+8 and their assembly into tetrasaccharide 'monomers' by 2+2 glycosylation. Reagents and conditions. (a) $PhCH(OMe)_2$, camphor sulfonic acid (CSA), dimethylformamide (DMF), 70%. (b) BnBr, dichloromethane (DCM), *n*-Bu_4NHSO_4, NaOH, aq. reflux, 23% **10**, 35% **21** (Supplementary Fig. 2). (c) **11**,TMSOTf, DCM, –20 °C. (d) 80% AcOH aq. 60 °C, 6 h, 75%. (e) Ac_2O, pyr., 93%. (f) NIS, Tf_2O, DCM/water (100:1, vol/vol), 62%. (g) CCl_3CN, 1,8-diazabicycloundec-7-ene (DBU), DCM, 45% **4**, 31% **7**. (h) FmocCl, pyr., overnight. (i) Ac_2O, pyr. (j) Et_3N, DCM, 57% for three steps. (k) (step 1) **14**, TMSOTf, DCM, –20 °C, 81%. (step 2) NaOMe, MeOH, 72%. (l) $PhCH(OMe)_2$, CSA, DMF, 50%. (m) 80% AcOH aq. 70 °C, 3 h. (n) Ac_2O, pyr., 69% over two steps. (o) (step 1) NIS, trifluoroacetic acid (TFA), DCM/water, 1 h; (step 2) CCl_3CN, DCM, DBU, 71% for two steps. (p) NaH, BnBr, DMF, 64%. (q) (step 1) NIS, TFA, DCM/water, 1 h; (step 2) CCl_3CN, DCM, DBU, 56% for two steps. (r) TMSOTf, $HSCHMe_2$, DCM, 65%. (s) Pd/C, H_2, 86%. (t) Butanedione, CSA, $CH(OMe)_3$, DCM, 35%. (u) TBSOTf, 2,6-lutidine, DCM, 99%. (v) TBSOTf, 2,6-lutidine, DCM, 99%. (w) TMSOTf, DCM, –20 °C. (x) TFA/water (9:1, vol/vol), 29% for two steps. (y) TBSOTf, 2,6-lutidine, DCM, 100%. (z) TMSOTf, DCM, –20 °C. See Supplementary Fig. 2 for additional details and compounds. Although different trichloroacetimidate anomers were used here (indicated by the added α and β symbols for the cartoon representations of **4** and **7**, respectively), there was no significant difference in the reactivity of anomers in these TMSOTf-activated '2+2' glycosylations, although the variation of conditions with other activators allowed variation of stereoselectivity (see main text).

triethylamine gave Gal acceptor **13**. Mannosylation of the free OH3 of **13** using donor **14** (ref. 30), bearing a participatory Ac ester at O2, at –20 °C promoted by TMSOTf gave Man-α-Gal disaccharide in good yield (81%) and with excellent alpha selectivity (>98%). This confirmed the designed compatibility of S^{i}Pr, the thioglycoside moiety in acceptor **13**, as a latent donor moiety that is inert under conditions suitable for trichloroacetimidate glycosylation activation. After glycosylation, selective protecting group manipulation gave the desired acceptor building block **5**. Notably, four Ac esters (Man *O*-2,3,4,6) were efficiently (72%) removed to yield **15** following treatment with a catalytic amount of sodium methoxide in methanol, while leaving the *O*-2 Ac ester of the Gal moiety intact. This remarkable transformation thereby allowed retention of the Ac ester that is critical for control of stereoselectivity in later polyglycosylation. Subsequent installation of a second benzylidene on the OH4,6 of the Man moiety gave **5**.

The second disaccharide acceptor **8** required for **K30-2** was assembled in turn from a Man thioglycoside acceptor and a Gal trichloroacetimidate donor (Supplementary Fig. 3c). Gal donor **16** was also accessed from IPTG **9** via the series of benzylidene and Ac ester installations established above. Thioglycoside hydrolysis then allowed direct preparation of trichloroacetimidate **16**. For Man acceptor **17**, the use of butane-2,3-diacetal (BDA) Frost–Ley protection[31] allowed selective access to the *cis* OH3,4 moiety needed for tetrasaccharide assembly. Although this could be used at an early stage in the preparation of **17**, more extensive purification was required, and a more efficient route with crystalline intermediates was instead adopted in which the BDA was installed subsequent to S^{i}Pr thioglycoside installation (Supplementary Fig. 3b). Regioselective protection of OH6 over OH2 using a bulky *tert*-butyldimethylsilyl ether in quantitative yield then gave Man acceptor **17**, in which OH2 was free, ready for glycosylation. Reaction of Gal donor **16** with Man acceptor **17** using TMSOTf as an activator proceeded smoothly without activation of the S^{i}Pr group in the acceptor (again confirming the designed S^{i}Pr strategy); this gave Gal-β-Man disaccharide **18** in good yield and good beta stereoselectivity (>98%) due to the participatory Ac ester at O2 of the Gal donor **16**. Subsequent protecting

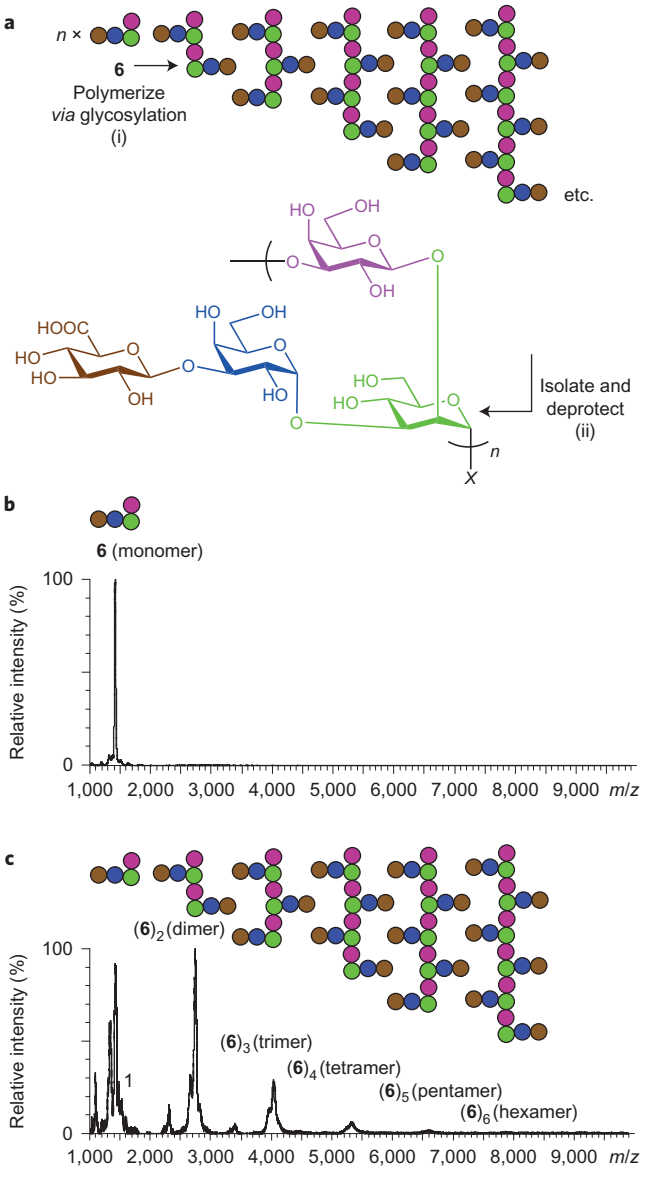

Figure 4 | Polyglycosylation of tetrasaccharide 'monomer' 6 for K30. **a**, Polyglycosylation of tetrasaccharide monomer **6** yielded **K30-2**$_{n=y}$ where $y = 1,2,3,4,5,6...$ Reagents and conditions: (i) NIS, TMSOTf, 3 h, −30 to −20 ° C, 55%; X = NHC(O)CH_2CH_2COOH, see Supplementary Section 'Characterization' for details. (ii) 0.5 N NaOH, MeOH-DCM, 1 day, 100%. **b**, MALDI-MS spectrum of 'monomer' **6**. **c**, MALDI-MS spectrum of the product of polyglycosylation shows a distribution with iterative increases in mass consistent with the expected polyglycosylation.

group manipulation allowed removal of the BDA to free OH3,4 in the Man moiety, thereby giving the final key disaccharide acceptor **8**.

Assembly of tetrasaccharide 'monomers' from the disaccharide building blocks. Encouraged by the successful compatibility of the S^{i}Pr thioglycosides as acceptors in disaccharide synthesis, we next tested this in the designed assembly of the **K30-1** and **K30-2** tetrasaccharide targets (Supplementary Figs 4–6). TMSOTf promoted the '2+2' glycosylation reaction of donor **4** and acceptor **5** to form tetrasaccharide **3** (protected **K30-1** 'monomer') in 35% yield, but only with poor regioselectivity; 26% of the corresponding *O*-2-glycosylated regioisomer was also isolated. Global three-step deprotection of **3** gave access to a single ($n = 1$) free tetrasaccharide K30 unit **K30-1**$_{n=1}$ bearing an S^{i}Pr reducing terminus β-thioglycoside in 46% overall yield.

The '2+2' glycosylation reaction with **7** and **8** towards the second desired **K30-2** tetrasaccharide monomer **6** proceeded with better regioselectivity than that to form **3**; the resulting yield of protected tetrasaccharide **19** (Supplementary Fig. 5) was an improved 45%. Notably, as intended (see above), no unwanted isopropylthiol aglycon transfer products were identified. Protecting group manipulation (cleavage of TBS ether and acetyl esters; further protection by acetyls and then Bn-ether hydrogenolysis) afforded the desired polymerizable tetrasaccharide **6** (protected **K30-2** 'monomer') in 49% overall yield. Global deprotection of **6** was straightforward; alkaline ester hydrolysis (OAc, OBz and OMe) in 0.5 N aqueous sodium hydroxide overnight allowed quantitative conversion to a single unit ($n = 1$) of K30-2 (**K30-2**$_{n=1}$), again bearing an S^{i}Pr reducing terminus β-thioglycoside.

Despite the complex nature of these assembled tetrasaccharides, their identities, configuration and connectivity (including, critically, the desired regioselective glycosylation sites) were confirmed by full characterization, including extensive one-dimensional and two-dimensional NMR (for example, clip-heteronuclear single quantum correlation (HSQC) and heteronuclear multiple band correlation (HMBC)) analysis. Interestingly, varying the conditions (Supplementary Section 'Methods and Characterization') also allowed access to variant 'unnatural' tetrasaccharides. Glycosylation of **4** with **5** activated by $BF_3{\cdot}OEt_2$ gave, exclusively, a product with a(n) (unnatural) beta linkage between the two disaccharides. Although not explored in this work, such tetrasaccharides highlight the potential to explore 'unnatural' synthetic polysaccharides that have been precisely altered (here α→β) at given repeating stereogenic centres.

Polyglycosylation. The '2+2' assembly strategies, vitally, preserved the S^{i}Pr moieties as latent donor groups. These could now be activated to serve as active donors in our polyglycosylation strategy (Fig. 2, polymerization point). Selective deprotection also revealed key acceptor hydroxyls, as intended, which should allow the reaction of each 'monomer' tetrasaccharide (**3** for K30-1 and **6** for K30-2) with another to allow polymerization/polyglycosylation (Fig. 4).

Polyglycosylation of both **3** and **6** was investigated through the activation of S^{i}Pr using *N*-iodosuccinimide (NIS)/TMSOTf as a promotor. These 'monomers' displayed strikingly contrasting reactivities. No K30-1 oligomers or polymers formed from **3** were detected. In contrast, polyglycosylation with **6** was highly successful. Indeed, **3** remained resistant under a range of conditions. It may be that, in this more congested 'monomer', access to the OH2 of the Man moiety is blocked by the glycosyl moieties at O1 (Gal) and O3 (Gal); the axial disposition of the OH2 acceptor will also reduce its accessibility and this may be exacerbated in a less conformationally flexible tetrasaccharide such as **3**.

The extent of polyglycosylation of **6** could be modulated by conditions. To create a low concentration of active electrophilic glycosylation intermediates, the promotor component TMSOTf was maintained at <1 equiv. in all reactions. Strict anhydrous conditions were maintained over the period of the reaction. To allow the more controlled growth of chains, polyglycosylation was also carried out at reduced temperature (−30 to −20 °C). Typical reaction times were on the order of hours (for example, 3 h). Reaction monitoring by matrix-assisted laser desorption ionization mass spectrometry (MALDI-MS) and characterization of immediate crude products confirmed the products of the polyglycosylation reaction and the occurrence of polymerization (Fig. 4). Products up to $n = 7$ (duodecaoctasaccharides) were routinely observed. Overall conversion of **6** to its oligomers or polymers was typically ~55%. The uniquely successful polymerization of the **K30-2** motif, as well as the more efficient '2+2' assembly of **6**, confirmed this as the preferred pathway for our approach.

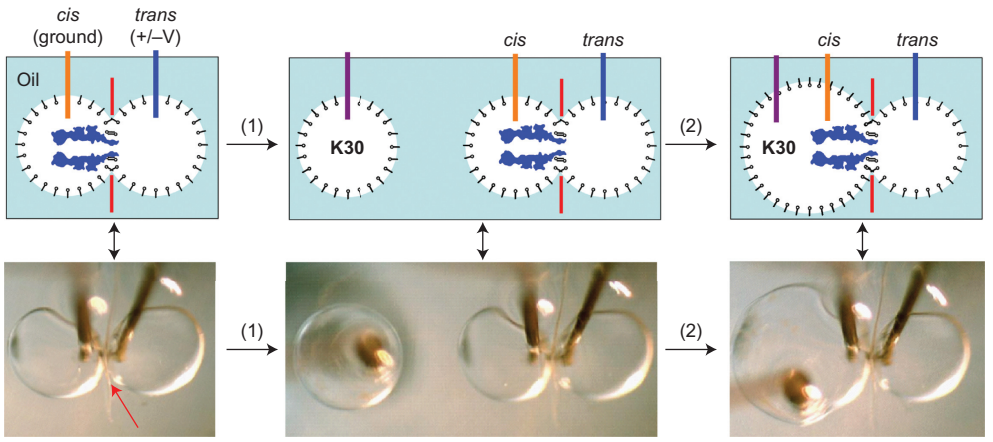

Figure 5 | Development of DIB-fusion system to allow analysis of the interaction between Wza pore ΔP106-A107 and K30 fragments K30-1$_{n=1}$, K30-2$_{n=1}$, K30-2$_{n=2}$ and K30-2$_{n=3}$. A three-droplet DIB-fusion system based on a bilayer interface between *cis* and *trans* droplets was constructed. An aperture (~200 μm in diameter) in the Teflon film (red and red arrow) restricts the size of the bilayer and provides stability. Oil is shown in light blue. Steps (1) and (2) show the fusion of a third droplet, containing the oligosaccharide substrate, to the *cis* droplet. The distance between the *cis* (orange) and *trans* (dark blue) electrodes was kept constant. The substrate droplet was fused with the *cis* droplet using a translational manipulator (purple) in the substrate droplet to mechanically drive the fusion process. The mutant Wza pore ΔP106-A107 (dark blue) was inserted into the lipid bilayer from the *cis* droplet (buffer, 300 mM KCl with 5 mM HEPES, pH 7.5).

Although these polymeric products could, in principle, after deprotection serve directly as a mixture of K30 substrates, we endeavoured to isolate and purify as many single components as possible. HPLC purification and MS analysis yielded the protected dimer and trimer of **6** (Supplementary Fig. 7). Global ester hydrolysis gave monodisperse K30-2 dimer (**K30-2**$_{n=2}$) and trimer (**K30-2**$_{n=3}$). These oligosaccharides could be fully characterized, despite their complexity (including by NMR (^{1}H, ^{13}C, 1D total correlation spectroscopy (TOCSY), HSQC, HMBC, HSQC coupled, nuclear Overhauser effect (NOE), 2D TOCSY), HRMS, infrared, optical rotation), thereby not only confirming their identity, but also, vitally, confirming the success of the polyglycosylation strategy in building such complex sugars. Products with higher numbers of repeating units, such as the tetramer, pentamer and hexamer of **6**, were detectable by MALDI-MS but could not be isolated in sufficient quantities and purities for full NMR analysis.

Development of the DIB-fusion system. We next sought to establish methods for the direct detection of the transport of the K30 sugar substrates through individual Wza translocons. Although the wild-type Wza protein shows a low unitary conductance, recently, in establishing a platform of assays for the development of novel anti-bacterial compounds, we reported[19] mutant Wza pores with conductance values representative of an open state. These Wza pores function in standard electrical planar bilayer systems, which were used here first to test transport activity. However, with these larger-volume systems, no events were detected with either of the tetramer sugar substrates **K30-1**$_{n=1}$ and **K30-2**$_{n=1}$, even at up to 1 mM concentration with the mutant Wza pore ΔP106-A107 (2 M KCl, buffered with 5 mM HEPES, pH 7.5).

The concentrations of sugars in this experimental set-up were limiting and prompted us to develop an improved interrogation system that would allow us to use higher concentrations. Previously, DIB systems have proven highly successful in allowing the manipulation of nanolitre volumes at both the *cis* and *trans* entrances of pores[20–24]. However, our attempts at the direct addition of analyte to the droplets (for example, by syringe) proved fruitless, leading only to mechanical disruption (DIB rupture). Therefore, to directly monitor Wza function before, during and after the introduction of sugar substrates, we designed a 'DIB-fusion' system for our measurements (Figs 1c and 5). This was achieved through the use of a third 'substrate droplet', containing mM concentrations of sugar, under the translational control of an independent micromanipulator, which was used to direct mechanical fusion with either the *cis* or *trans* droplet, as desired.

Thus, a single copy of the 'open' mutant Wza pore ΔP106-A107 was first established and maintained in the DIB bilayer (Fig. 5 and Supplementary Fig. 8). A Teflon film with an aperture was located between the *cis* and *trans* droplets to increase the stability of the bilayer. Specifically, after insertion of a single Wza pore ΔP106-A107 from the *cis* droplet into the bilayer, K30 substrate was added to either the *cis* droplet or the *trans* droplet through fusion to give a final concentration of ~10 mM. When tested in the DIB-fusion format, the interactions of **K30-1** and **K30-2** fragments with Wza ΔP106-A107 were successfully detected (Supplementary Figs 9 and 10). Moreover, interaction events were evident only when the substrate was added to the *cis* droplet but not the *trans* droplet, consistent with the previously proposed orientation of Wza with respect to the biosynthetic machinery for K30 in bacteria[6].

The events were next compared with those gained from a heterogeneous, natural sample of K30 (Supplementary Fig. 11). A sample of K30 oligosaccharides (sugar residues ≥4, that is, approximately equivalent to or greater in size than **K30**$_{n=1}$) was created through direct acidic hydrolysis, monitored by ^{1}H NMR, of a sample of natural K30 obtained by electrophoretic separation (see Supplementary Methods and Supplementary Figs 12 to 14) and added to the *cis* droplet by fusion. No interaction events were observed between the Wza pore ΔP106-A107 and intact (0 min of hydrolysis or initially hydrolysed for 10 min), full-length natural **K30** CPS (50 μg ml^{-1}). By contrast, interaction events similar to those observed using shorter, pure synthetic K30 fragments were observed from natural **K30** CPS that had been hydrolysed to shorter lengths for 30–240 min (Supplementary Fig. 11).

Single-molecule recapitulation of Wza-K30 CPS export. Although the pure synthetic K30 fragments are shorter than the full-length K30 polysaccharide, these initial qualitative observations of transport events are highly encouraging. We therefore sought to use the longer pure fragments derived through polyglycosylation as defined substrates for more detailed, quantitative measurements of sugar transport.

Four representative fragments of K30 CPS (**K30-1**$_{n=1}$, **K30-2**$_{n=1}$, **K30-2**$_{n=2}$ and **K30-2**$_{n=3}$) were examined. In DIB-fusion experiments, both **K30-2**$_{n=1}$ and **K30-1**$_{n=1}$ showed interaction events

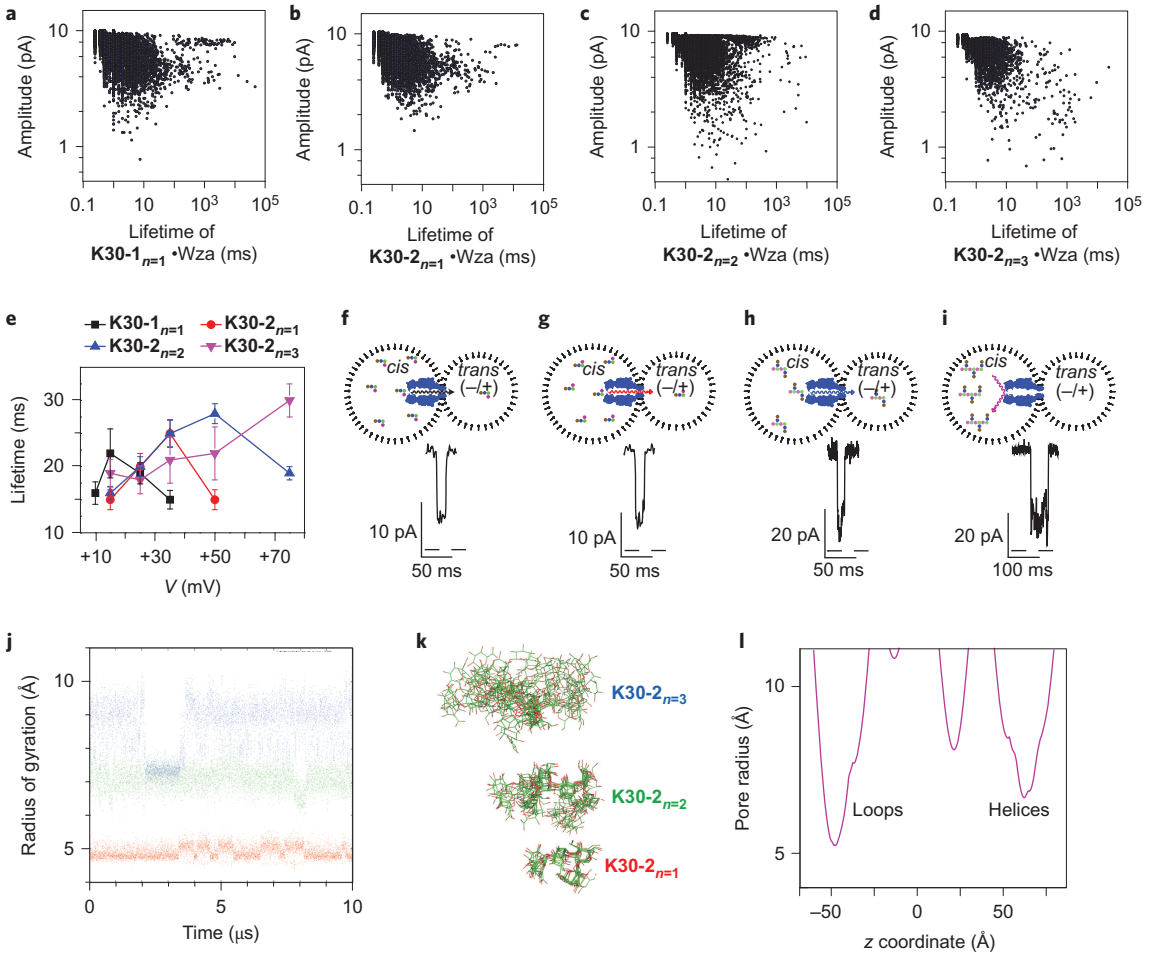

Figure 6 | Analysis of the interaction between Wza pore ΔP106-A107 and K30 fragments K30-1$_{n=1}$, K30-2$_{n=1}$, K30-2$_{n=2}$ and K30-2$_{n=3}$ using the DIB-fusion system. a–d, Scatter plots of mutant Wza pore ΔP106-A107 interaction with **K30-1$_{n=1}$** (10 mM), **K30-2$_{n=1}$** (100 mM), **K30-2$_{n=2}$** (5 mM) and **K30-2$_{n=3}$** (1 mM) in 300 mM KCl buffer at +25 mV, respectively. **e**, Lifetimes of **K30-1$_{n=1}$** (black, 10 mM), **K30-2$_{n=1}$** (red, 100 mM), **K30-2$_{n=2}$** (blue, 5 mM) and **K30-2$_{n=3}$** (purple, 1 mM) associated with the mutant Wza pore ΔP106-A107 versus the applied potential. Each point is derived from the mean of three experiments and the standard deviation (s.d.) is shown (mean ± s.d., $n = 3$) **f–i**, Representative interaction events of **K30-1$_{n=1}$** (**f**), **K30-2$_{n=1}$** (**g**), **K30-2$_{n=2}$** (**h**) and **K30-2$_{n=3}$** (**i**) with mutant Wza pore ΔP106-A107 in 300 mM KCl buffer. The volume of each droplet was ~200 nl. The applied electrical potential was +35, +50, +75 and +75 mV, respectively. Dashed line shows 0 pA. The sampling rate was 5 kHz (filtering 1 kHz). Note that events are less frequent for lower concentrations of sugar substrate but the lifetimes analysed here are independent of concentration. **j**, Radii of gyration of **K30-2$_{n=1}$** (red), **K30-2$_{n=2}$** (green) and **K30-2$_{n=3}$** (blue) predicted by MD simulation. **k**, Aligned simulated conformers of **K30-2$_{n=1}$**, **K30-2$_{n=2}$** and **K30-2$_{n=3}$**. Ten predicted conformers of each substrate were aligned. Each conformer was generated after every 1 μs in a 10 μs continuous molecular dynamics simulation. **l**, Pore radii of Wza pore ΔP106-A107 determined with HOLE (ref. 19).

with the Wza pore (Fig. 6a,b,f,g and Supplementary Figs 15 and 16) when measured in 300 mM KCl, buffered with 5 mM HEPES, pH 7.5 over a range of concentrations (10, 50 and 100 mM **K30-2$_{n=1}$** and 7.5, 10, 50 and 100 mM **K30-1$_{n=1}$**). **K30-2$_{n=2}$** (5 mM) and **K30-2$_{n=3}$** (1 mM) also exhibited observable interaction events (Fig. 6c,d and Supplementary Figs 17–19).

Importantly, the DIB-fusion system allowed the first estimates of the mean lifetimes of interaction and/or transport complexes to be obtained using pure sugar substrates. As expected, the lifetimes (Supplementary Figs 15, 16, 18 and 19) are independent of substrate concentration. Notably, despite the varied structures of the sugar substrates, all showed similar lifetimes at +25 mV (**K30-1$_{n=1}$**·Wza ΔP106-A107, **K30-2$_{n=1}$**·Wza ΔP106-A107, **K30-2$_{n=2}$**·Wza ΔP106-A107 and **K30-2$_{n=3}$**·Wza ΔP106-A107 are 19 ± 2 ms ($n = 3$ pores), 20 ± 2 ms ($n = 3$ pores), 20 ± 2 ms ($n = 3$ pores) and 18 ± 2 ms ($n = 3$ pores), respectively; Fig. 6e, Supplementary Figs 15–19 and Supplementary Methods). These preliminary results suggest that the initial interaction of Wza with sugar is not obviously a critically rate-limiting event, based on structure, and that if sugar size does have an effect, it is slight.

To examine whether these events represent transport processes, we also obtained the lifetimes of the complexes of K30 substrates (**K30-1$_{n=1}$**, **K30-2$_{n=1}$**, **K30-2$_{n=2}$** and **K30-2$_{n=3}$**) and the Wza pore ΔP106-A107 under different applied potentials. The lifetimes of the smaller sugars (four to eight residues) displayed a dependency on voltage with maxima as follows: **K30-1$_{n=1}$** at +15 mV (22 ± 4 ms); **K30-2$_{n=1}$** at +35 mV (25 ± 2 ms) and **K30-2$_{n=2}$** at +50 mV (28 ± 2 ms) (Fig. 6e, Supplementary Figs 15–19). The lifetimes decreased significantly when the applied potential was higher than the maxima, indicating the transport of the K30 substrates from the *cis* droplet to the *trans* droplet through the Wza pore (Fig. 6e–h). This is consistent with the overall negative charge at pH 7.5 of the K30 substrates; increased positive applied potential gives a stronger driving force, which pushes the substrates through the pore[19,32–35]. An increased potential difference drives more rapid transport. As a comparison, we added the blocker am$_8$γCD to the *cis* side via droplet fusion and observed the same phenomenon[19]. Am$_8$γCD binds to the transmembrane α-helix barrel. An increased negative applied potential drove the positively charged am$_8$γCD through the pore when

the applied potential was more negative than −20 mV (Supplementary Fig. 20).

In contrast to the smaller sugars, the lifetimes for the 12-mer **K30-2**$_{n=3}$ did not exhibit a maximum, even up to an applied potential of +75 mV, suggesting that the dodecamer is too hindered to be electrophoretically driven through the pore, despite the much higher applied potential (Fig. 6e and Supplementary Figs 17b–i and 19). In addition, permanent blockades were observed at high applied potentials (≥50 mV) with **K30-2**$_{n=3}$. Reversal of the applied potential was required to reopen the pore following such a blockade (Supplementary Fig. 19f), consistent with an encounter event with **K30-2**$_{n=3}$ that leads to an unsuccessful attempt to translocate.

Together, these data, and critically the observed voltage dependencies, suggest that **K30-1**$_{n=1}$, **K30-2**$_{n=1}$ and **K30-2**$_{n=2}$ can be translocated through the Wza pore ΔP106-A107 above certain positive applied potentials, while **K30-2**$_{n=3}$ is too encumbered to pass through the pore. Interestingly, the frequency of all interaction events when normalized by concentration (directly proportional to the 'on' rate; see Supplementary Methods) was greater for greater displayed overall charge, for example, **K30-2**$_{n=3}$ > **K30-2**$_{n=2}$ > **K30-2**$_{n=1}$ (measured at pH 7.5 where the carboxylic acid group of every repeating 4-mer unit would be expected to be negatively charged, Supplementary Fig. 21). This suggested that the capture ('on') rate for initial encounter events may also be charge-dependent.

Molecular dynamics analysis of K30 CPS. Prompted by these intriguing data, we conducted explicit solvent molecular dynamics (MD) simulations of K30 CPS oligomers of increasing length, **K30-2**$_{n=1}$, **K30-2**$_{n=2}$ and **K30-2**$_{n=3}$ (Supplementary Section 'Methods'). These were performed[36] over extended periods (10 μs) using a method with ACEMD[37] software running on highly parallel graphics processing units. These experiments revealed that the predicted dominant radii of gyration for these three substrates are 4.5–5.5 Å, 6.0–8.0 Å and 7.0–10.0 Å, respectively (Fig. 6j). The greatly different flexibilities of these substrates can also be visualized in the overlaid aligned conformers taken every 1 μs during the simulations (Fig. 6k). **K30-2**$_{n=1}$ is the least flexible and most compact, and **K30-2**$_{n=3}$ is the most flexible. The Wza pore has a narrow but flexible entrance (5.2 Å) and a rigid exit (6.7 Å) for K30 CPS (Fig. 6l and Supplementary Fig. 22). Comparison of these radii and the radii of the K30 CPS substrates suggests a consistent mechanistic model (supported by the translocation–voltage experiments described above) in which both **K30-2**$_{n=1}$ (4.5–5.5 Å) and **K30-2**$_{n=2}$ (6.0–8.0 Å) are capable of adopting conformers that may translocate, although this will be more difficult for **K30-2**$_{n=2}$ (supported by the requirement of a higher electric applied potential for translocation to occur, that is, maximum lifetimes at +50 mV versus +35 mV). In contrast, **K30-2**$_{n=3}$ conformers appear to be too large to translocate.

Discussion

We have shown here a single-molecule recapitulation of K30 export to examine the interactions between a membrane pore, Wza and precise fragments of its natural sugar substrates. These K30 oligosaccharides and polysaccharides were obtained by an unusual approach for the chemical synthesis of such complex structures—polymerization of an activated hybrid donor–acceptor tetrasaccharide monomer unit. We propose a step-growth polymerization mechanism in which chain ends are not capped or terminated (the nucleophile is permanently exposed). This leads to continual (rather than 'burst' and terminate[15]) growth to give better access to longer polymers. These proof-of-principle examples have accessed only modest lengths by the standards of polymerization (up to 28-mers in good conversion with ~55% total isolable yield of all polymeric products), but in so doing we have created some of the most complex examples of CPS oligosaccharides made to date. The isolation of discrete, pure oligosaccharides highlights strongly that, even with modest success, important complex structures may be accessed through this approach. The likely key to a general application of this approach, as we show here, will involve the evaluation of differing minimum repeating units that may deliver the same polymeric product. It has been a frequent bias that only one of the possible repeating ('monomer') units, typically the most synthetically accessible, is selected for synthesis. This bias could lead to complete failure not only in chemistry but also in the discovery of biology. Here, we show that open-minded selection is vital to success.

Furthermore, our *in vitro* recapitulation of sugar transport reveals mechanistic information about Wza-mediated sugar export. Notably, the addition of the sugar substrate to the extracellular side of the Wza transporter pore did not generate any blockades, whereas clear interactions between the periplasmic end of the Wza pore (Fig. 1) and the K30 oligosaccharides were observed. These observations serve to confirm the interaction asymmetry of Wza and imply that the pore is inherently 'chemically rectified' to prevent any significant inhibitory rebinding by CPS post-transport from the extracellular space, even without the help of the extracellular lectin Wzi, which is thought to sequester CPS once transported[7]. It is possible, for example, that this 'rectification' originates from inherent chemical bias created by the internal cavity and the extracellular end of Wza that together may act akin to the 'greasy slide' suggested for maltoporin channels[32,38]. It is notable that although transport could be 'driven' by an increasing potential difference in the correct direction, interactions in the opposing (anti-export) direction were not observed (Supplementary Fig. 9). This tight control may be exerted electrostatically by the 16 negatively charged residues (8× E369 + 8× Y373) found in the constriction site on the extracellular *trans* side of Wza. This strong local electrostatic gradient may prove significant, because the global potential across the outer membrane of *E. coli* is low, at <7 mV (inside negative) in >300 mM NaCl (ref. 39), and, as we have shown here, is insufficient to force transport in the export direction. In turn, this may be further potentiated and/or regulated by other membrane proteins in the transport complex such as the transmembrane tyrosine kinase Wzc, whose function is in turn adjusted by the cytoplasmic cognate phosphatase Wzb (refs 2–5,40).

The similar lifetimes with the Wza pore that we have measured here for different K30 CPS structures and fragment lengths and types also imply that the initial interaction with Wza is not obviously rate-limiting in transport. Thus, a model may be developed in which Wzy and Wzc combine to build and introduce/push CPSs, unit by unit, to the 'bottom' of the Wza 'bottle'. These units, when driven, slip readily into the bottle as a result of the interactions suggested above. The lack of selectivity for differently ordered fragments (that is, K30-1 versus K30-2) further supports this notion and suggests that this is a continuous 'pushing' process that does not require a particular 'ratchet' motif to be formed before a translocation event into the bottle occurs. We suggest that dodecamers are 'too long' (perhaps too conformationally 'jumbled') to slip into Wza, and this is supported by the radii of gyration determined through MD analysis and their correlation with the pore size of Wza. This, in turn, suggests that careful coordination of biosynthesis and transport (and hence Wzy, Wzc and Wza) is required to maintain CPS in a conformationally manageable state suitable for transport. It should be noted, of course, that the data and observations obtained here for shorter oligomers cannot necessarily be extrapolated to far longer fragments that will be present in the natural system.

By combining these first pure CPS substrates with a nanolitre-scale measurement approach (the DIB-fusion system), the interactions of even very small amounts of synthesized glycans could be tested at high concentrations (>10 mM). Previous bilayer

systems proved unsuitable, because they required larger volumes[19], and the use of operationally more complex chip/syringe methods[25] cannot maintain protein pores during substrate addition[20–24]. Precious synthetic materials (derived from multi-step syntheses) with even weak affinity can now be used to probe and quantitatively analyse protein–sugar interactions. Given the typical complexity and difficulty of glycan assembly and the general weakness of many sugar–protein interactions, we believe that these combined approaches, which feature a ready approach to the synthesis (trivially named 'poly-go-saccharides') and the use of very small quantities of synthetic product (applied here to study sugar transport), could find far-reaching applications in numerous vital binding processes in glycobiology.

Received 11 December 2014; accepted 24 February 2016; published online 18 April 2016

References

1. Lebeer, S., Vanderleyden, J. & De Keersmaecker, S. C. Host interactions of probiotic bacterial surface molecules: comparison with commensals and pathogens. *Nature Rev. Microbiol.* **8,** 171–184 (2010).
2. Bushell, S. R. *et al.* Crystallization and preliminary diffraction analysis of Wzi, a member of the capsule export and assembly pathway in *Escherichia coli*. *Acta Crystallogr. F* **66,** 1621–1625 (2010).
3. Cuthbertson, L., Mainprize, I. L., Naismith, J. H. & Whitfield, C. Pivotal roles of the outer membrane polysaccharide export and polysaccharide copolymerase protein families in export of extracellular polysaccharides in Gram-negative bacteria. *Microbiol. Mol. Biol. Rev.* **73,** 155–177 (2009).
4. Dong, C. *et al.* Wza the translocon for *E. coli* capsular polysaccharides defines a new class of membrane protein. *Nature* **444,** 226–229 (2006).
5. Whitfield, C. Biosynthesis and assembly of capsular polysaccharides in *Escherichia coli*. *Annu. Rev. Biochem.* **75,** 39–68 (2006).
6. Nickerson, N. N. *et al.* Trapped translocation intermediates establish the route for export of capsular polysaccharides across *Escherichia coli* outer membranes. *Proc. Natl Acad. Sci. USA* **111,** 8203–8208 (2014).
7. Bushell, S. R. *et al.* Wzi is an outer membrane lectin that underpins group 1 capsule assembly in *Escherichia coli*. *Structure* **21,** 844–853 (2013).
8. Willis, L. M. & Whitfield, C. Structure, biosynthesis, and function of bacterial capsular polysaccharides synthesized by ABC transporter-dependent pathways. *Carbohydr. Res.* **378,** 35–44 (2013).
9. Micoli, F. *et al.* Development of a glycoconjugate vaccine to prevent meningitis in Africa caused by meningococcal serogroup X. *Proc. Natl Acad. Sci. USA* **110,** 19077–19082 (2013).
10. Adamo, R. *et al.* Synthetically defined glycoprotein vaccines: current status and future directions. *Chem. Sci.* **4,** 2995–3008 (2013).
11. Boltje, T. J., Buskas, T. & Boons, G.-J. Opportunities and challenges in synthetic oligosaccharide and glycoconjugate research. *Nature Chem.* **1,** 611–622 (2009).
12. Wang, L.-X. & Davis, B. G. Realizing the promise of chemical glycobiology. *Chem. Sci.* **4,** 3381–3394 (2013).
13. Hudak, J. E. & Bertozzi, C. R. Glycotherapy: new advances inspire a reemergence of glycans in medicine. *Chem. Biol.* **21,** 16–37 (2014).
14. Hungerer, D., Jann, K., Jann, B., Orskov, F. & Orskov, I. Immunochemistry of K antigens of *Escherichia coli*. 4. The K antigen of *E. coli* O9:K30:H12. *Eur. J. Biochem.* **2,** 115–126 (1967).
15. Schuster, H. J., Vijayakrishnan, B. & Davis, B. G. Chain-growth polyglycosylation: synthesis of linker-equipped mannosyl oligomers. *Carbohydr. Res.* **403,** 135–141 (2015).
16. Kochetkov, N. K., Betaneh, V. I., Ovchmmkov, M. V. & Backmowsky, L. V. Synthesis of the O-antigenic polysaccharide of *Salmonella newington* and of its analogue differing in configuration at the only glycosidic centre. *Tetrahedron* **37,** 149 (1981).
17. Kochetkov, N. K. Tetrahedron report number 218: synthesis of polysaccharides with a regular structure. *Tetrahedron* **43,** 2389–2436 (1987).
18. Nifantiev, N. E., Backmowsky, L. V. & Kochetkov, N. K. Synthesis of the capsular polysaccharide of *Streptococcus pneumoniae* type 14. *Bioorg Khzm (USSR)* **13,** 273 (1987).
19. Kong, L. *et al.* Single-molecule interrogation of a bacterial sugar transporter allows the discovery of an extracellular inhibitor. *Nature Chem.* **5,** 651–659 (2013).
20. Fischer, A., Holden, M. A., Pentelute, B. L. & Collier, R. J. Ultrasensitive detection of protein translocated through toxin pores in droplet-interface bilayers. *Proc. Natl Acad. Sci. USA* **108,** 16577–16581.
21. Holden, M. A., Needham, D. & Bayley, H. Functional bionetworks from nanoliter water droplets. *J. Am. Chem. Soc.* **129,** 8650–8655 (2007).
22. Hwang, W. L., Chen, M., Cronin, B., Holden, M. A. & Bayley, H. Asymmetric droplet interface bilayers. *J. Am. Chem. Soc.* **130,** 5878–5879 (2008).
23. Hwang, W. L., Holden, M. A., White, S. & Bayley, H. Electrical behavior of droplet interface bilayer networks: experimental analysis and modeling. *J. Am. Chem. Soc.* **129,** 11854–11864 (2007).
24. Syeda, R., Holden, M. A., Hwang, W. L. & Bayley, H. Screening blockers against a potassium channel with a droplet interface bilayer array. *J. Am. Chem. Soc.* **130,** 15543–15548 (2008).
25. Lein, M., Huang, J. & Holden, M. A. Robust reagent addition and perfusion strategy for droplet-interface bilayers. *Lab Chip* **13,** 2749–2753 (2013).
26. Li, Z. & Gildersleeve, J. C. Mechanistic studies and methods to prevent aglycon transfer of thioglycosides. *J. Am. Chem. Soc.* **128,** 11612–11619 (2006).
27. Kato, M., Hirai, G. & Sodeoka, M. Studies on the selectivity between glycosylation and intermolecular aglycone transfer of thioglucoside in synthesis of lactose derivatives. *Chem. Lett.* **40,** 877–879 (2011).
28. Cheng, L., Chen, Q., Liu, J. & Du, Y. Synthesis of a fluorescence-labeled K30 antigen repeating unit using click chemistry. *Carbohydr. Res.* **342,** 975–981 (2007).
29. Bazin, H. G., Wolff, M. W. & Linhardt, R. J. Regio- and stereoselective synthesis of β-D-gluco-, α-L-ido-, and α-L-altropyranosiduronic acids from Δ(4)-uronates. *J. Org. Chem.* **64,** 144–152 (1999).
30. Matsuo, I., Isomura, M., Miyazaki, T., Sakakibara, T. & Ajisaka, K. Chemoenzymatic synthesis of the branched oligosaccharides which correspond to the core structures of *N*-linked sugar chains. *Carbohydr. Res.* **305,** 401–413 (1997).
31. de Kort, M. *et al.* Synthesis of potent agonists of the D-myo-inositol 1,4,5-trisphosphate receptor based on clustered disaccharide polyphosphate analogues of adenophostin A. *J. Med. Chem.* **43,** 3295–3303 (2000).
32. Kullman, L., Winterhalter, M. & Bezrukov, S. M. Transport of maltodextrins through maltoporin: a single-channel study. *Biophys. J.* **82,** 803–812 (2002).
33. Dumas, F., Koebnik, R., Winterhalter, M. & Van Gelder, P. Sugar transport through maltoporin of *Escherichia coli*: role of polar tracks. *J. Biol. Chem.* **275,** 19747–19751 (2000).
34. Sanchez-Quesada, J., Ghadiri, M. R., Bayley, H. & Braha, O. Cyclic peptides as molecular adapters for a pore-forming protein. *J. Am. Chem. Soc.* **122,** 11758–11766 (2000).
35. Gu, L.-Q., Cheley, S. & Bayley, H. Capture of a single molecule in a nanocavity. *Science* **291,** 636–640 (2001).
36. Sattelle, B. M. & Almond, A. Shaping up for structural glycomics: a predictive protocol for oligosaccharide conformational analysis applied to *N*-linked glycans. *Carbohydr. Res.* **383,** 34–42 (2014).
37. Harvey, M. J., Giupponi, G. & Fabritiis, G. D. ACEMD: accelerating bio-molecular dynamics in the microsecond time-scale. *J. Chem. Theory Comput.* **5,** 1632–1639 (2009).
38. Schirmer, T., Keller, T. A., Wang, Y. F. & Rosenbusch, J. P. Structural basis for sugar translocation through maltoporin channels at 3.1 Å resolution. *Science* **267,** 512–514 (1995).
39. Nikaido, H. Molecular basis of bacterial outer membrane permeability revisited. *Microbiol. Mol. Biol. Rev.* **67,** 593–656 (2003).
40. Collins, R. F. *et al.* The 3D structure of a periplasm-spanning platform required for assembly of group 1 capsular polysaccharides in *Escherichia coli*. *Proc. Natl Acad. Sci. USA* **104,** 2390–2395 (2007).
41. Bohne, A., Lang, E. & von der Lieth, C. W. W3-SWEET: carbohydrate modeling by internet. *J. Mol. Model.* **4,** 33–43 (1998).
42. Bohne, A., Lang, E. & von der Lieth, C. W. SWEET—WWW-based rapid 3D construction of oligo- and polysaccharides. *Bioinformatics* **15,** 767–768 (1999).

Acknowledgements

The authors thank the Medical Research Council and the Engineering and Physical Sciences Research Council for financial support. L.K. has received a Wellcome Trust VIP award and a UK/China Postgraduate Research Scholarship. B.G.D. was a Royal Society Wolfson Research Merit Award recipient during this work.

Author contributions

L.K., H.B. and B.G.D. designed the experiments. L.K. performed the experiments. A.A. designed, performed and analysed the MD simulations. L.K., H.B. and B.G.D. analysed the results. L.K., H.B. and B.G.D. wrote the paper. All authors discussed the results and commented on the manuscript.

Additional information

Supplementary information is available in the online version of the paper. Reprints and permissions information is available online at www.nature.com/reprints. Correspondence and requests for materials should be addressed to H.B. and B.G.D.

Competing financial interests

The authors declare no competing financial interests.